A diffused-interface model for the lyophilization of a packed bed of spray-frozen particles

A diffused-interface model for the lyophilization of a packed bed of spray-frozen particles

*Lorenzo Stratta, Merve B. Adali, Antonello A. Barresi, Gianluca Boccardo, Agnese Marcato, Raffaele Tuccinardi, Roberto Pisano**

Molecular Engineering Laboratory, Department of Applied Science and Technology, Politecnico di Torino, 24 corso Duca degli Abruzzi, IT-10129 Torino, Italy.

*** Corresponding Author**

E-mail: roberto.pisano@polito.it

ABSTRACT.

Spray freeze-drying is particularly suitable for the preservation of biopharmaceuticals as it involves gentle drying and can easily be integrated with continuous manufacturing strategies. This process is still an evolving application, and its potential is often being explored experimentally. However, experimental methods are expensive and time-consuming. Therefore, much effort is currently focused on the development of mathematical models to understand the basic mechanisms and hence lay the foundation for analysis and experimentation. Even though a few models were proposed in the past, all of them presented various flaws and failed in describing the process behavior. We propose a multiscale approach, which is able to reproduce the structure of a packing of spray-frozen particles and extract detailed pore-scale geometrical features, informing the final vial-scale drying and heat transfer simulation. This latter step is the main innovation here presented, a new model that is based on the concept of a diffused interface and describes the process in a more accurate way.

Keywords: Spray freeze drying; diffused interface; multiscale; particles.

1. INTRODUCTION

The last decades have been a time of great innovation and evolution in the pharmaceutical industry, which was recently transformed by the advent of biopharmaceuticals such as recombinant proteins, monoclonal antibodies, RNA-based therapeutics, etc. Biopharmaceuticals have flooded the market of life-savings drugs[1] as the *small molecules* cannot compete in potency, efficacy, and reduced side effects[2]. Unfortunately, these bioproducts have a short shelf-life if stored as liquid solutions and cannot undergo conventional, hot drying processes because of their temperature sensibility. Consequently, freeze-drying is generally utilized, allowing the increase in the shelf-life of biomolecules without altering their structure and therapeutic activity. However, freeze-drying is an inefficient and expensive process[3] that strongly relies on batch manufacturing and may represent an unacceptable bottle-neck in a condition of high urgency. The recent Covid-19 pandemic showed the world how freeze-drying, instead of low-temperature storage at -80°C, could have saved both time and money in the production and distribution of vaccines; furthermore, the application of continuous technologies would have made the manufacturing plants more prompt to answer to sudden variations in the market request. Recently, the pharmaceutical industry showed interest in continuous manufacturing technologies to modernize its production chain[4–9]. Among the various continuous technologies, spray freeze-drying (SFD) is of great interest as a particle manufacturing method that involves converting temperature-sensitive solutions into dried particles. The main idea behind SFD is to create a particle-based product and, thus, increase the sublimating surface area, resulting in shorter processing times[10,11]. Although SFD has so far been carried out as a batch process, it could potentially be converted into a continuous one[12,13]. An accurate description of the heat and mass transfer phenomena occurring during the lyophilization of particle-based products can make this transition easier. This mathematical model can also

support professionals in selecting appropriate drying conditions and promote process optimization. In the literature, a few models have already been proposed for the SFD process[14–16], but they do not accurately describe the drying behavior within a packed-bed of frozen particles. In this paper, we developed a mechanistic model based on the concept of a diffused interface to describe the drying dynamics and heat transfer at the scale of the vial. This vial-scale simulation is supported by an *in-silico* workflow composed of other computational models which can describe the structure of the frozen material at smaller spatial scales. Specifically, starting from experimental data of the frozen particle size distribution, we can reconstruct a geometrical model of the packing, which is then used to obtain detailed structural parameters, both from image analysis post-processing and ad-hoc fluid dynamics simulations. This data is then used to inform and enrich the vial-scale model, whose performance then shows how such an integrated, multiscale approach provide a more realistic description of the freeze-drying of packed-beds of frozen particles. This multiscale workflow is shown in Figure 1.

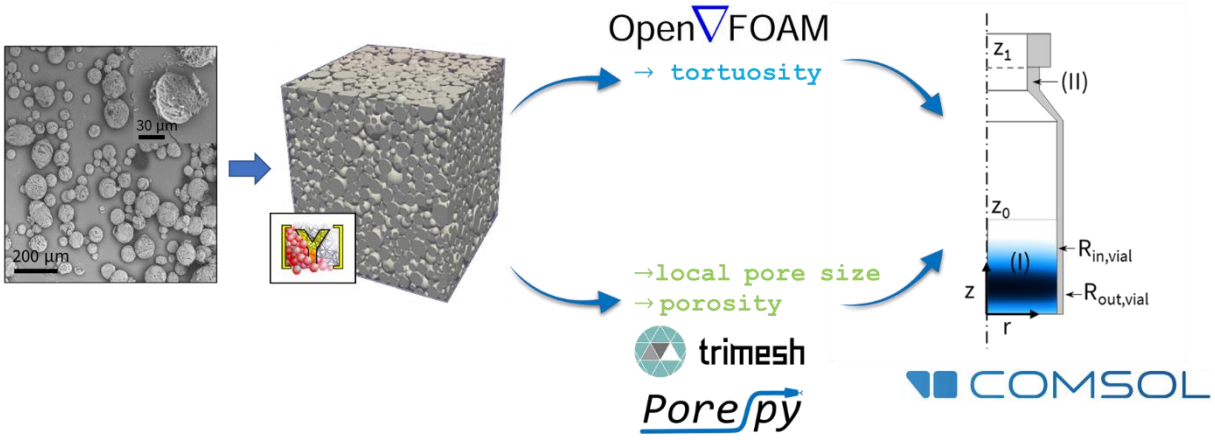

Figure 1. Multiscale modeling workflow used in the present study for the description of the SFD process.

2. MATHEMATICAL MODEL

2.1.PRE-EXISTING MODELS

In 2009, Liapis and Bruttini[14] developed the first mechanistic model for the lyophilization of a packed-bed of frozen particles. Taking inspiration from what has been proposed for the freeze-drying of bulk products, the authors proposed a pseudo-homogenous model where the packed-bed of particles is approximated to a two-layer system; dried and frozen layers separated by a moving sublimation interface. The dusty-gas model[17] describes the mass transport within the two layers, and a dimensionless variable, i.e., the ice saturation S, provides the state of progress of the separation. The ice saturation is the fraction of the ice volume to the pore volume in the particle and, thus, is zero in the dried layer. Unlike the models proposed for the bulk products, a generation term is added in the continuity equation to account for the sublimation or re-condensation of water vapor. The moving sublimation interface is then treated as a Stefan problem, and the energy balance at the interface determines its velocity.

Capozzi et al.[15,16] integrated this pseudo-homogenous model in a multiscale platform, which includes the generation of random packings of spherical particles and their characterization in terms of permeability, tortuosity, and porosity through a Computational Fluid Dynamics (CFD) analysis.

In both models, the description of the system is inaccurate; in a packed bed of particles being lyophilized, there is no clear separation between fully and partially dried regions as it occurs in the conventional freeze-drying of bulk products where the sublimation front separates the system into two distinct subdomains. Moreover, equilibrium conditions are assumed in the frozen layer, i.e., the local water partial pressure corresponds to the ice vapor pressure. However, this assumption is

correct only if the mass transport resistance inside the single particles is negligible compared to that of the packed-bed, and this situation rarely occurs in SFD.

2.2.DIFFUSE INTERFACE MODEL

In this section, a pseudo-homogeneous model based on the diffuse interface approach is proposed. In a packed bed of frozen particles, ice sublimation occurs within the entire system and its rate locally depends on the water partial pressure. A physical sublimating interface is clearly present within individual particles, whereas there is no clear separation within the packed bed. The position of the sublimating interface within the particles can be transferred on the macroscopic scale through an intensive variable S. Unlike the model proposed by Liapis and Bruttini[14], the packed bed is no more divided into two separate domains, i.e., the dried and the frozen layer; it contains a unique domain wherein S describes the state of progress of sublimation. A physical separation between thoroughly dried and partially dried particles can still be present and detected through a more or less steep gradient of S. In the following sections, the mathematical formulation at the macroscopic and particle scales of this model is given.

2.2.1. MACROSCOPIC DESCRIPTION

The following description refers to the lyophilization of particles in vials, but the model formulation is valid independently of the type of containers, e.g., trays, syringes, and blisters. However, in the case of vials, we can take advantage of axial symmetry; it follows that a 2D axisymmetric model can accurately describe the drying behavior within the packed bed, making computational costs less challenging. Nonetheless, the model equations are generally valid, whichever is the 3D geometry to be described. In the following part we refer to the system geometry shown in Figure 2.

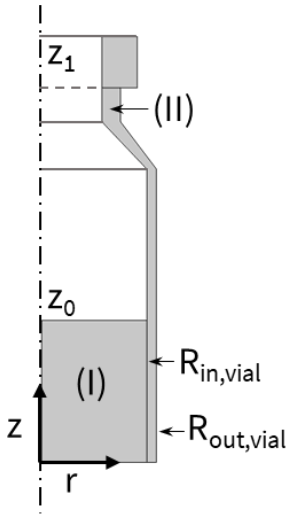

Figure 2. Schematic of the packed bed of particles (I) contained within a vial (II). The axis of rotation is depicted as the dash-dot line. The bottom of the vial is not simulated as its contribution is already included in the heat transfer coefficient K_v'. The z axis has its origin at the bottom of the product and the r axis at the centre of the vial.

The energy balance for the vial domain is

$$\rho_{vial} c_{p,vial} \frac{\partial T_{vial}}{\partial t} + \nabla(-k_{vial} \nabla T_{vial}) = 0 \tag{1}$$

The subscript *vial* refers to the vial material (e.g., Borosilicate glass) while ρ, c_p, and k refer respectively to the density, specific heat, and thermal conductivity. The boundary condition is the continuity of temperature at the interface between the vial wall and the packed bed ($r = R_{in,vial}$). Furthermore, we can assume that the vial side-wall is adiabatic:

$$\nabla T = 0\,, \qquad r = R_{out,vial} \tag{2}$$

The heat transfer through the vial side-wall is negligible since in the experimental setup used the vials are tightly packed and, apart from the few at the edge of the batch, all the vials are

approximately at the same temperature. Thus, it is reasonable to assume that almost no heat is transferred from vial to vial and from the environment to the vial side-wall.

At the top of the vial, heat is transferred from the shelf above through radiation:

$$-\mathbf{n} \cdot (-k_{vial} \nabla T_{vial}) = \sigma F_{1,2} \left(\varepsilon_{shelf,rad} T_{shelf}^4 - \varepsilon_{vial,rad} {T_{vial}}^4 \right), \qquad \forall r, z = Z_1 \tag{3}$$

where σ is the Stefan-Boltzmann constant, $\varepsilon_{shelf,rad}$ and $\varepsilon_{vial,rad}$ are respectively the emissivities of the shelf and vial, and $\mathbf{n}$ is the normal versor of the surface. Moreover, the view factor is considered equal to 1. This assumption is reasonable if the upper shelf is close enough to the top of the vials, which often occurs in conventional freeze-drying.

The ice-saturation within the packed bed, S, is locally defined as the ratio between the amount of sublimated ice and the initial ice content:

$$S = 1 - \frac{C_{ice,sub}}{C_{ice,0}} \tag{4}$$

The initial ice content, $C_{ice,0}$, corresponds to the initial amount of ice per unit volume of the packed bed:

$$C_{ice,0} = \frac{(1 - \varepsilon_{bed}) \varepsilon_p \rho_{ice}}{M_w} \tag{5}$$

where ε_{bed} is the bed (subscript *bed*) porosity, ε_p the particles (subscript *p*) porosity, and M_w the water (subscript *w*) molecular weight. Given these two definitions, S has a value of 1 at the beginning of primary drying and 0 when the particles are completely dried. However, values greater than 1 are allowed in the case of vapor condensation on the particles' surface. The maximum allowed value of S is imposed by the system's geometry and will be further discussed later on.

The energy balance in the product domain reads:

$$\rho_{bed} c_{p,bed} \frac{\partial T_{bed}}{\partial t} = \nabla(k_{bed} \nabla T_{bed}) - c_{p,gas}\big(\nabla(\mathbf{N}_t T_{bed})\big) + \dot{Q} \tag{6}$$

where $\dot{Q}$ is the volumetric heat generation due to phase change and the term $\mathbf{N}_t$ represents the mass flux in the porous matrix. The physical properties of the packed bed as a homogenous medium are defined as a linear combination of the properties of the frozen (subscript *f*) and dried (subscript *d*) particles and of the gas (subscript *gas*) occupying the inter-particles empty space, weighted on their corresponding volume:

$$c_{p,bed} = (1 - \varepsilon_{res})\big[c_{p,f} S + c_{p,d}(1 - S)\big] + \varepsilon_t c_{p,gas} \tag{7.1}$$

$$k_{bed} = (1 - \varepsilon_{res})\big[k_f S + k_d(1 - S)\big] + \varepsilon_t k_{gas} \tag{7.2}$$

$$\rho_{bed} = (1 - \varepsilon_{res})\big[\rho_f S + \rho_d(1 - S)\big] + \varepsilon_t \rho_{gas} \tag{7.3}$$

where ε_{res} corresponds to the porosity of the bed, ε_{bed}, when S<1, and is corrected to account for the space occupied by the ice in the event of vapor condensation on the particles' surface when S>1:

$$\varepsilon_{res} = \begin{cases} \varepsilon_{bed} & ,S < 1 \\ \varepsilon_{bed} + (1 - \varepsilon_{bed})\varepsilon_p(1 - S) & ,S \geq 1 \end{cases} \tag{8}$$

The physical properties of the frozen and dried particles are approximated as a linear combination of the properties of the solid excipient (subscript *s*) and ice (subscript *ice*) or interstitial gas (subscript *gas*). The frozen particles are thus so described:

$$c_{p,f} = c_{p,s}\big(1 - \varepsilon_p\big) + c_{p,ice}\varepsilon_p \tag{9.1}$$

$$k_f = k_s\big(1 - \varepsilon_p\big) + k_{ice}\varepsilon_p \tag{9.2}$$

$$\rho_f = \rho_s\big(1 - \varepsilon_p\big) + \rho_{ice}\varepsilon_p \tag{9.3}$$

and similarly for the dried ones, substituting the subscript *ice* with the subscript *gas*.

At $z = Z_1$, the vial receives a heat flux from the upper shelf by radiation. Part of this heat flux is then transferred by conduction through the vial wall and part by radiation to the product.

Assuming a view factor equal to 1 between the top of the vial and the product, the boundary condition at the top of the packed bed is

$$-\mathbf{n}\cdot(-k_{bed}\nabla T_{bed}) = \sigma\left(\varepsilon_{vial,rad}T_{vial}^4 - \varepsilon_{bed,rad}T_{bed}^4\right), \qquad r < R_{in,vial}\,, z = Z_0 \tag{10}$$

At the bottom of the packed bed, heat is transferred from the shelf through various mechanisms and can be described as

$$-\mathbf{n}\cdot(-k_{bed}\Delta T_{bed}) = K_v'\left(T_{shelf} - T_{bed}\right), \qquad \forall r, z = 0 \tag{11}$$

where K_v' is the overall heat transfer coefficient between the shelf and the bottom of the product which can be estimated by theoretical calculations or experimentally determined (see Pisano et al.[18]). The overall heat transfer coefficient K_v' can be described as a function of the chamber pressure P_c

$$K_v' = A_1 + \frac{A_2 P_c}{1 + A_3 P_c} \tag{12}$$

If K_v' is experimentally determined by a gravimetric test[19] like in this work, its measurement accounts for all the contributions to heat transfer, including the radiation contribution coming from the upper shelf and heat conducted by the vial wall, and should be corrected according to the characteristics of the model in which it is employed, as discussed by Velardi and Barresi[20]. In this work a 2D model including the wall is adopted, with the contribution by radiation explicitly described in Eq. (11), thus it is necessary to subtract such a contribution from K_v'. A 40% reduction was calculated to account for this contribution. This result is coherent with what has been previously estimated in the literature[5].

The term $\dot{Q}$ in equation (6), the heat generation related to the ice sublimation or condensation, is calculated as:

$$\dot{Q} = -G_w \Delta H_s M_w \tag{13}$$

where ΔH_s is the ice heat of sublimation and G_w is the volumetric ice sublimation rate (or vapor condensation rate) expressed in mol $m^{-3}s^{-1}$. The total mass flux in the porous matrix, $\mathbf{N}_t$, is calculated as the sum of the water vapor ($\mathbf{N}_w$) and inert gas ($\mathbf{N}_{in}$) mass fluxes:

$$\mathbf{N}_t = \mathbf{N}_w + \mathbf{N}_{in} \tag{14}$$

These mass fluxes can be estimated through to the Dusty Gas Model (DGM) as:

$$\mathbf{N}_i = \frac{M_i}{RT}(c_1 \nabla p_i + c_2 y_i \nabla P + c_3 p_i \nabla P) \tag{15}$$

where the subscript i stands for either water vapor or inert gas, while the total pressure P is the sum of the water and inert partial pressures, respectively p_w and p_{in}, R is the gas constant, y_i the i-species molar fraction and c_1, c_2 and c_3 are described as:

$$c_1 = \frac{D_i^{Kn} D_{i,j}^{eff}}{D_{i,j}^{eff} + y_i D_j^{Kn} + y_j D_i^{Kn}} \tag{16.1}$$

$$c_2 = \frac{D_i^{Kn}\left(D_{i,j}^{eff} + D_j^{Kn}\right)}{\left(D_{i,j}^{eff} + y_i D_j^{Kn} + y_j D_i^{Kn}\right)} \tag{16.2}$$

$$c_3 = \frac{B_{0,b}}{\mu_{gas}}\left(1 + \frac{\varepsilon_{bed}}{(1-\varepsilon_{bed})\varepsilon_p} - S\right) \tag{16.3}$$

where μ_{gas} is the gas viscosity, and $B_{0,b}$ the bed permeability. The three coefficients respectively account for Knudsen diffusion, bulk binary diffusion, and viscous flow (described with the Darcy's law). The effective diffusivities are

$$D_i^{Kn} = \frac{\varepsilon_{res}}{\tau^2}\frac{d_{pore,bed}}{3}\sqrt{\frac{T}{\pi M_i}} \tag{17.1}$$

$$D_{i,j}^{eff} = \frac{\varepsilon_{res}}{\tau^2} D_{i,j} \tag{17.2}$$

$$D_{i,j} = 0.2315 \left(\frac{T}{T_*}\right)^{2.5595} \left(\frac{p_*}{p}\right) \tag{17.3}$$

where $T_* = 273.15\ K$, $p_* = 101325\ Pa$[21] and $d_{pore,bed}$ is the average pore diameter of the bed. This quantity is described in section 2.3.1.

Knowing $\mathbf{N}_w$ and $\mathbf{N}_{in}$ it is possible to solve the mass transport equations:

$$\frac{\partial(\varepsilon_{res} C_w)}{\partial t} = -\nabla \mathbf{N}_w + G_w \tag{18.1}$$

$$\frac{\partial(\varepsilon_{res} C_{in})}{\partial t} = -\nabla \mathbf{N}_{in} \tag{18.2}$$

with a no-flux boundary condition at the packed bed-vial interface:

$$\mathbf{n} \cdot (\nabla \mathbf{N}_i) = 0\,, \qquad r = R_{in,vial}\,, \forall z \tag{19}$$

The boundary conditions at the top of the packed bed are defined using commonly observed values in conventional freeze-drying:

$$C_{w,top} = \frac{0.95\ P_c}{RT}\,, C_{in,top} = \frac{0.05\ P_c}{RT}, \qquad r < R_{in,vial}\,, z = Z_0 \tag{20}$$

In the proposed model, while it is possible to obtain values of S>1, it is never possible to obtain values of S with no physical meaning. When $S = S_{critical} = f(\varepsilon_{bed})$ (e.g., there is enough ice condensed between the particles to fill up all the empty space), $\varepsilon_{res} = 0$, $c_1 = c_2 = c_3 = 0$, $\boldsymbol{N}_i = \boldsymbol{N}_j = 0$ and, therefore, also $\boldsymbol{N}_t = 0$ and in equation (18.1) $\partial(\varepsilon_{res} C_w)/\partial t = 0$. The block of ice impedes the mass flux, and no more ice can condensate. This intrinsic stop condition mimics the system's behavior and prevents unrealistic situations.

The initial condition within the packed bed is defined assuming equilibrium between ice and water vapor at the initial temperature T_0:

$$C_{w,0} = \frac{p^0_{ice}(T_0)}{\mathrm{R}T_0}\,, \qquad r < R_{in,vial}\,, z < Z_0 \tag{21}$$

The term G_w in equations (13) and (18.1) can instead be evaluated assuming a local non-equilibrium between the ice-vapor equilibrium pressure at the particles sublimating interface, p_{ice}^0 and the concentration of water vapor in the empty inter-particle space.

$$G_w = \begin{cases} \left(\frac{p_{ice}^0(T)}{RT} - C_w\right) v_s \ , if \left(\frac{p_{ice}^0(T)}{RT} - C_w\right) \geq 0 \\ \left(\frac{p_{ice}^0(T)}{RT} - C_w\right) v_c \ , if \left(\frac{p_{ice}^0(T)}{RT} - C_w\right) < 0 \end{cases} \quad (22)$$

where v_s and v_c are functions describing the sublimation and condensation kinetics and will be discussed later on. The equilibrium partial pressure of water can be expressed with the Marti-Mauersberger relationship[22]:

$$\log_{10}(p_{ice}^0) = \frac{-2663.5}{T} + 12.537 \quad (23)$$

If, at a certain temperature, the local water vapor concentration is lower than the equilibrium concentration, ice in the particles tends to sublimate and G_w assumes positive values, while condensation occurs if there is an excess of water vapor in the space surrounding the particles, and G_w becomes negative. Sublimation and condensation are two distinct phenomena and can follow different kinetics. Therefore, they have been here described by introducing two separate kinetic variables, v_s and v_c. In this paper, these parameters were estimated through a mathematical model that describes the sublimation of individual particles, see next section.

Once the generation term G_w is defined, its time integration provides the local amount of sublimated (or condensed) ice, which is then used to determine S in equation (4):

$$C_{ice,sub} = \int_0^t G_w dt \quad (24)$$

2.2.2. DRYING OF INDIVIDUAL PARTICLES

The value of the kinetic parameters v_s can be estimated by the description of an individual spherical particle of radius R_0. The particle is divided into dried (subscript *d*) and frozen (subscript *f*) layers, separated by a moving sublimating interface. The energy balance within the dried and frozen layers are

$$\rho_d c_{p,d} \frac{\partial T_d}{\partial t} = \nabla(k_d \nabla T_d) - \rho_{vgas} c_{p,gas} \mathbf{u} \cdot \nabla T_d \tag{25.1}$$

$$\rho_f c_{p,f} \frac{\partial T_f}{\partial t} = \nabla\left(k_f \nabla T_f\right) \tag{25.2}$$

The physical properties are defined as already discussed in Eq. (9), while the boundary condition at the outer particle's surface is

$$-\mathbf{n} \cdot (-k_d \nabla T_d) = q\,, \qquad r = R_0 \tag{26}$$

If we assume that the particles are in direct contact with the interior of the vial bottom, the average heat flux at the external surface q can be roughly estimated from the heat flux from the shelf, Q_{shelf}:

$$q = \frac{Q_{shelf}}{S_p N_p} \tag{27.1}$$

$$Q_{shelf} = K_v' \, S_{vial}\left(T_{shelf} - T_{vial,bottom}\right) \tag{27.2}$$

where S_p and S_{vial} are respectively the external surface of the individual particle and the horizontal section of the vial. K_v' is the overall heat transfer coefficient between the heating shelf and the packed bed bottom. The number of particles in direct contact with the vial bottom, N_p, is proportional to both S_p and S_{vial}. There are several ways of calculating this value with different levels of accuracy, e.g., rectangular arrangement of the particles, hexagonal arrangement, extraction from simulations of randomly packed beds. In this study, the rectangular arrangement

was used because it provides a reasonable approximation of the real system, while being very easy to calculate.

$$N_p = \frac{\pi D R_{in,vial}^2 (1-\varepsilon_s)}{\pi R_0^2} = \frac{\pi R_{in,vial}^2}{4R_0^2} \tag{28.1}$$

$$\varepsilon_s = \frac{4R_0^2 - \pi R_0^2}{4R_0^2} = 1 - \frac{\pi}{4} \tag{28.2}$$

In the dried layer, for simplicity, only water vapor is considered for the gas phase and the mass transport is then defined as:

$$\varepsilon_p \frac{\partial \rho_w}{\partial t} + \nabla(\rho_w \mathbf{u}) = 0 \tag{29}$$

and, the superficial gas velocity, is calculated with the Darcy equation:

$$\mathbf{u} = \frac{B_{0,p}}{\mu_{gas}} \nabla P \tag{30}$$

where the permeability is calculated with the Carman-Kozeny equation:

$$B_{0,p} = \frac{d_{pore}^2}{180} \frac{\varepsilon_p^3}{\left(1-\varepsilon_p^2\right)} \tag{31}$$

The pressure of the chamber, P_c, is set to be both the boundary condition at the particle surface and the initial condition in the dried domain. The presence of the inert is here not considered sensibly reducing the complexity of the system. This assumption is reasonable given that the concentration of the inert will always be smaller than 5% inside the packed bed.

The moving interface is described as a Stefan problem, and the heat balance equation can be solved with an infinitely thin interface (subscript *int*):

$$-\Delta H_s \mathbf{N}_{w,int} + \mathbf{n}_{int} \cdot \left(-k_f \nabla T_f\right) - \mathbf{n}_{int} \cdot \left(-k_d \nabla T_d\right) = 0 \tag{32}$$

Combining Eq. (32) with the water continuity equation, we obtain

$$-\mathbf{n}_{int} \cdot \mathbf{N}_{w,int} = \mathbf{v}_{int} \rho_{ice} \varepsilon_p \tag{33}$$

Substituting Eq. (33) in Eq. (32), the velocity of the moving interface results

$$\mathbf{v}_{int} = \frac{\mathbf{n}_{int} \cdot \left(-k_f \nabla T_f\right) - \mathbf{n}_{int} \cdot \left(-k_d \nabla T_d\right)}{\Delta H_s \rho_{ice} \varepsilon_p} \tag{34}$$

In calculating the temperature gradients, the interface temperature is set equal to the ice vapor temperature calculated through Eq. (23).

The kinetic parameter v_s can eventually be calculated integrating the mass flux over the interface surface S_{int} :

$$v_s = \frac{\oiint \mathbf{n}_{int} \cdot \mathbf{N}_{w,int} dS_{int}}{\left(\frac{p_{int}}{RT_{int}} - \frac{P_c}{RT_{r=R_0}}\right) M_w V_{ref}} \tag{35.1}$$

$$V_{ref} = \frac{{}^4\!/_3 \, \pi R_0^3}{1 - \varepsilon_{bed}} \tag{35.2}$$

As the dried layer thickness increases, the resistance to the mass transport inside the particle increases along with the pressure driving force and, therefore, the kinetic parameter reduces. The value of v_s is, therefore, an implicit function of the ice saturation S (both are function of time and can be correlated trough this variable), and, once this relationship is defined, it can be used in the macroscopic description of the packed bed of particles.

2.3. MODEL PARAMENTERS DEFINITION AND CASE STUDIES

2.3.1. PACKED BED POROSITY, PERMEABILITY, AND TORTUOSITY

The structures resulting from the spray freeze-drying process were reproduced in-silico as a packing of spherical particles in order to characterize the packed bed computationally. The packing was designed imposing the particle size distribution resulting from the experimental sample described in section §2.3.2.

- Creation of the packed bed

The discrete element method (DEM) implemented in Yade[23] was employed for the sedimentation simulation of the particles. In the simulations, the initial configuration is a cloud of spheres, subjected to gravity, depositing in a box. As a result, a realistic packing of spheres is obtained.

Each particle in the box interacts with the neighboring particles. These interactions are modeled by a non-cohesive elastic-frictional contact model[24]. In the DEM simulations, the contact force between two spheres is given by two contributions: the normal force and the shear force. In this modeling approach, the particles are allowed to overlap at the contact point and the overlap depth depends on the materials Young's module. The normal force arises from a difference of linear velocity along the interaction axis, and reads as follows:

$$F_N = K_N u_N \tag{36}$$

where u_N is the normal displacement and K_N is the normal interaction stiffness, defined as:

$$K_N = 2\frac{E_i r_i \, E_j r_j}{E_i r_i + E_j r_j} \tag{37}$$

where $E_{i,j}$ is the Young's modules of the particles materials and $r_{i,j}$ is the radius of the spheres. If $u_N \geq 0$ the normal force is null, so the interactions between spheres that are not in contact are not considered in the model.

The shear force arises from the perpendicular component of the linear velocities difference and the perpendicular component of rotational velocities summation. It is defined in the same way with the corresponding shear stiffness and displacement:

$$F_T = K_T u_T \tag{38}$$

where K_T is a function of K_N according to the Poisson's law. A check is performed on the shear force in order to follow the Coulomb friction law, which imposes a maximum limit equal to $F_N \tan(\phi)$, where ϕ is the friction angle between the two particles.

Given the forces, the DEM code integrates the motion equation for each particle. Starting from the position of a specific sphere, $\mathbf{x}_p(t)$, the code calculates the position after the time step Δt, $\mathbf{x}_p(t+\Delta t)$, integrating the Newton's second law for translation and rotation:

$$m_p \frac{\partial^2 \mathbf{x}}{\partial t^2} = \sum_{i=0}^{n_C} \left(\mathbf{F}_{i,p}^N + \mathbf{F}_{i,p}^T\right) + m_p \mathbf{g} \tag{39.1}$$

$$I_p \frac{\partial \boldsymbol{\omega}}{\partial t} = \sum_{i=0}^{n_C} \left(\left(\mathbf{F}_{i,p}^T\right) \times r_p(\mathbf{n})\right), \tag{39.2}$$

where m_p is the particle mass, $\mathbf{g}$ is the gravitational acceleration, n_C is the number of contact points, $\mathbf{F}_{i,p}^N, \mathbf{F}_{i,p}^T$ are the normal and shear components of the contact force between a couple of particles, I_p is the moment of inertia, r_p is the distance between the contact point and the center of the particle and $\mathbf{n}$ is the contact plane normal versor.

At the end of this simulation, the result is a random collection of objects (i.e. spheres) packed by sedimentation, but this is not yet the final geometry to be employed in the CFD simulation. In fact, the YADE simulation boundaries (the walls of the sedimentation box) cause a distortion of the local positioning of the spheres which, if ported to a simulation meant to represent a small representative sample of a volume of packed freeze-dried grain, would result in an unphysical representation. For this reason, in order to get rid of these unwanted wall effects, a subsequent procedure of "cutting" was performed to obtain a reduced Representative Elementary Volume (REV).

There is of course the matter of keeping the statistical significance of this reduced volume in terms of representation of the original particle size distribution, to be balanced with high computational costs of using larger volumes in the CFD simulation. The concept of a REV is a well-studied issue in the field of porous media[25] and the specifics of its evaluation for the construction of appropriate CFD models was tackled in our previous work, where more details can be found[26]. A visualization of both the end-result of the YADE simulation and the extracted REV can be found in Figure 3.

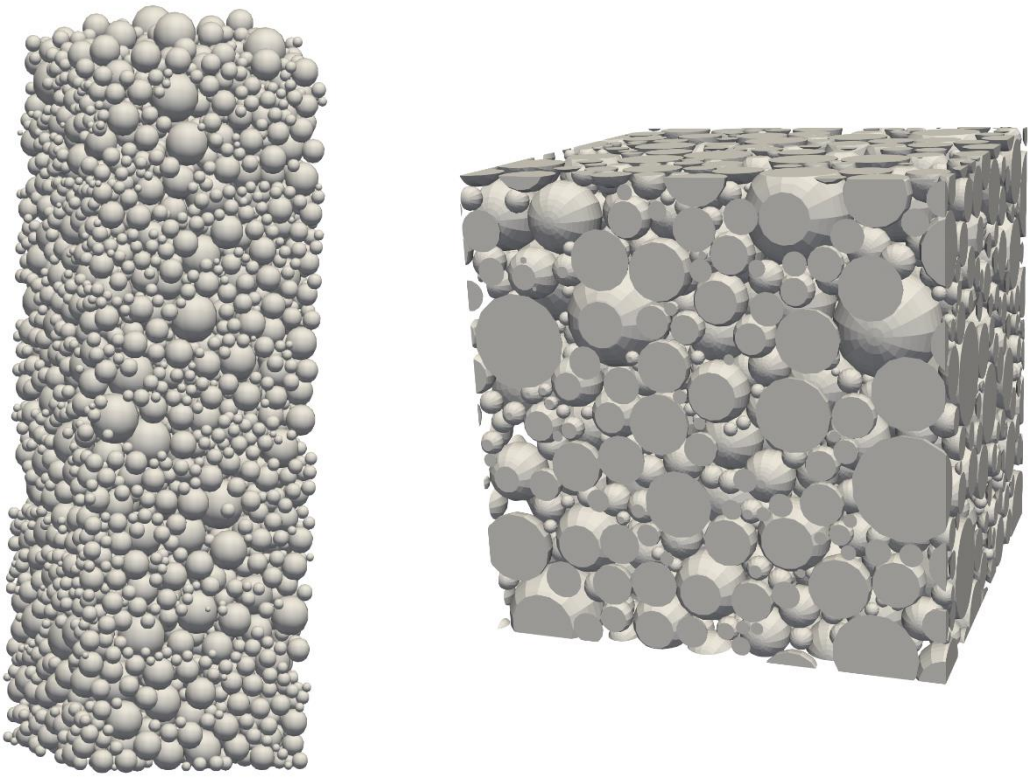

Figure 3. Sphere packing as resulting from the YADE simulation (left), and the extracted Representative Elementary Volume (right).

Then, these representative volumes of the packings created via DEM simulations can be analyzed in terms of tortuosity, permeability, porosity, and average pore size diameter, by using these geometries in CFD simulations.

- CFD simulations of the packed bed

The tortuosity is evaluated CFD simulations of flow in the packings. The open-source toolbox OpenFOAM v7 was employed. The flow inside the packings is simulated in laminar conditions; the fluid considered is water modeled as an incompressible Newtonian fluid at 25°C with kinematic viscosity, ν, equal to $0.89 \cdot 10^{-6}$ $m^2 s^{-1}$. The solver simpleFoam, that implements the SIMPLE algorithm, is used to solve the continuity and Navier-Stokes equations:

$$\nabla \cdot \mathbf{U} = 0 \tag{40.1}$$

$$\frac{D\mathbf{U}}{Dt} = -\frac{1}{\rho}\nabla p + \nu \nabla^2 \mathbf{U} \tag{40.2}$$

where $\mathbf{U}$ is the fluid velocity, p is the fluid pressure and ρ is the fluid density. Also in this case, the reader interested in more in-depth exploration of the numerical details of these simulations is referred to one of our previous works[27] where a similar setup was employed.. There are a number of different ways which can be used to estimate the tortuosity of the porous medium when the detailed local geometry is available[28,29]. Using only the flow field obtained from a CFD simulation, it is easy to extract this parameter that can be defined as the ratio between the volume integral of the velocity in the main direction of flow and the magnitude of the velocity[29,30]:

$$\tau = \frac{\int U_x dV}{\int \|\mathbf{U}\| dV} \tag{41}$$

From the same flow field, it is possible to obtain the bed permeability too. The surface velocity of the fluid can be calculated as:

$$U_S = \|\mathbf{U}\| \frac{A_S}{A_T} \tag{42}$$

where A_S and A_T are the fluid surface (averaged over the bed height) and the total section surface of the simulated packed bed, respectively. Knowing the pressure drop across the simulated portion of the bed, it is possible to calculate the bed permeability, $B_{0,bed}$, from the Darcy equation.

From the mesh used to simulate the packed bed tortuosity and permeability, it is possible to calculate the bed porosity as:

$$\varepsilon_{bed} = \frac{V_{tot} - V_p}{V_{tot}} = \frac{V_{mesh}}{V_{tot}} \tag{43}$$

where V_{tot} is the total volume of the box containing the particles, V_p is the total volume occupied by the particles and V_{mesh} is the volume of the meshed region outside the spheres.

One of the advantages of reproducing *in-silico* the geometries of the chosen packings of freeze-dried granules (and of pore-scale modeling in general) is the possibility to explore more than just integral and averaged quantities, such as porosity, tortuosity, or permeability. Specifically, from the geometry obtained in the previous step from the DEM simulation it is possible to extract the full distribution of the sizes of the pores in any given packing.

The pore size distribution (represented in Figure 4 for the case of a 5% (w/w) mannitol solution) is the probability density function of the dimensions of the voids in a porous medium. This analysis is performed by using the Python's library PoreSpy[31] which requires as input rasterized images. We, therefore, used the library Trimesh to operate the voxelization of the geometries created via DEM. The binary images we created in this way contain 0 in the solid phase and 1 in the pore phase.

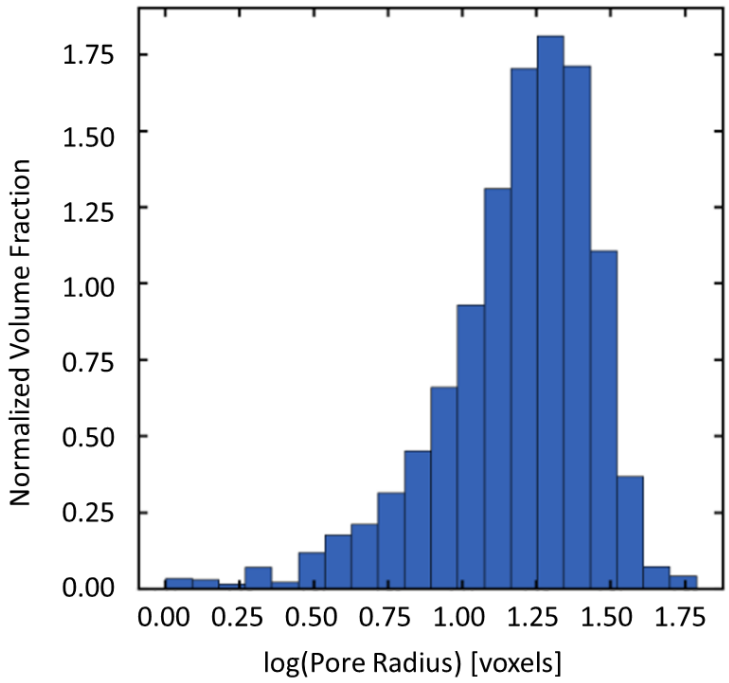

Figure 4. Pore Size Distribution of the packing geometry corresponding to 5% (w/w) mannitol solution, with feed flow rate of 5 mL/min. The pore sizes (i.e. radii) are given in terms of voxels, the working unit for PoreSpy post-processing operation.

The approach implemented in PoreSpy consists in finding which voxel can accommodate a sphere of a given radius. Given the number of sizes and the bins in the size distribution, the algorithm detects the largest pore by applying the Euclidean distance transform to the image. After that, the algorithm looks for all the smaller spheres between 0 and the largest one by using the Fast Fourier Transform convolution. Naturally, from the pore size distribution it is possible to calculate the mean dimension of the pores, $d_{pore,bed}$, which while being an integral and averaged value, it will be in this case a more precise and quantitative estimation of the characteristic length relevant for the involved pore-scale transport phenomena, more useful with respect to e.g. the more classical assumption of equating the mean size of the pores to the mean size of the granules, which becomes less accurate especially in the cases of strongly poly-disperse distributions, such as the one under consideration.

Another advantage of a fully *in-silico* workflow for the extraction of geometrical feature information from experimental data and evaluation of the relevant transport parameters is its repeatability, allowing for a robust and consistent analysis of wide datasets.

In this work, we have chosen to focus on a specific combination of excipient type, concentration, liquid flow rate, and atomization power, the details of which are given in a previous publication[32].

Lastly, the parameters extracted from these analyses (i.e. τ, $B_{0,bed}$, ε_{bed} and $d_{pore,bed}$), and used in the following COMSOL simulations, are listed in Table 1.

2.3.2. PRODUCTION OF SPRAY FREEZE-DRIED PARTICLES AND PARTICLE DIAMETER DETERMINATION

SFD process is described by three major steps: atomization, spray-freezing, and freeze-drying. Spray-frozen particles are produced by spraying a feed solution from an atomizer into a cryogenic medium, commonly liquid nitrogen. The frozen particles are then collected and freeze-dried to sublimate the ice[12]. The atomizer used to spray the liquid solution produces spherical, porous particles with a size in the micrometer range, which results in a great specific surface and, therefore, high water evaporation rate[33–35].

In this study, spray freezing into vapor over liquid nitrogen followed by lyophilization was used to produce mannitol powder. A 5% (w/w) mannitol (≥98%, Sigma-Aldrich-Fluka, Buchs, Switzerland) solution prepared in water for injection (Fresenius Kabi, Verona, Italy) was sprayed into a dewar containing liquid nitrogen by a 60 kHz ultrasonic atomizer (Buchi, Switzerland) at 3 W input power from approximately 7 cm above the surface of the liquid nitrogen. The volumetric flow rate of 5 mL/min at which the solution was fed to the atomizer was controlled using a syringe pump (KDS 200 model, KD Scientific, Holliston, MA). The frozen particles were collected and transferred into 10R glass vials with a 24 mm outer diameter and a 22 mm internal diameter. The

vials were filled with the frozen particles to a bed height of 15 mm. The freeze-drying cycle was carried out using MicroFD® (Millrock Technology, Kingston, NY, USA). Primary drying was performed at 10°C and 15 Pa, while secondary drying was conducted at 20°C for 5 h and the dried powders in vials were stored at -20°C until further analysis. The endpoint of primary drying was determined by monitoring the 2 pressure profiles (Pirani gauge and capacitance monometer)[36] and calculating the onset and offset times. The onset time refers to the point at which the Pirani gauge starts to decrease, while the offset time is when Pirani to capacitance monometer ratio is equal to 1, which indicates the end of primary drying. The onset time was determined as the intersection of the tangents through the primary drying plateau and the decreasing zone of Pirani curve, as shown in Figure 5a. The onset time was found at around 15.3 h and the offset was found approximately at 24 h, considering the initial 1.5 h taken to reach appropriate shelf temperature for frozen particles (Figure 5a). The difference between the offset time and the onset time might be due to the vial-to-vial heterogeneity within the batch, i.e., the sublimation behavior of the various vials within the batch was different. The product temperature was measured using T-type thermocouples placed in the bottom center of vials and their readings are shown in Figure 5b.

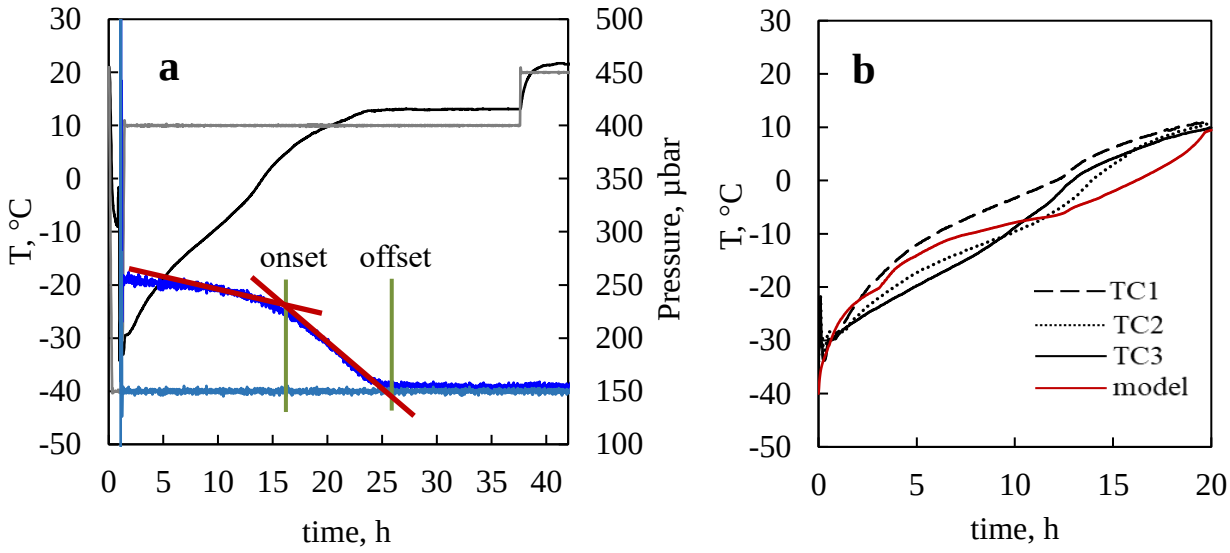

Figure 5. a) Freeze-drying cycle of 5% (w/w) mannitol particles, showing onset and offset times, shelf temperature (gray), procuct temperature (black), Pirani gauge pressure (dark blue), and capacitance manometer pressure (light blue) **b)** Comparison of product temperature between the output of thermocouples (TC) and the model prediction.

The particle morphology and shape were characterized using scanning electron microscopy (SEM) (Phenom XL, Phenom-World B.V., Netherlands). ImageJ software (National Institute of Health, USA) was used to calculate the particle size distribution by randomly selecting 200-300 particles from the SEM images. The particle morphology and particle size distribution are shown in Figure 6. The black line corresponds to the lognormal distribution fit, giving an average particle size of 32.5 μm and a standard deviation of 12.1 μm. The internal pore size of the product was also analysed using the SEM image of the internal structure of a single particle (Figure 6) that was found to be cut in half. This quantitative analysis was achieved by selecting 60 pores and each of them was assumed to be an ellipse, and the pore size was then calculated as the diameter of the circle with the same area-to-circumference ratio of the assumed ellipse. The SFD particle had an internal average pore diameter of 2.36 ± 0.47 μm.

The average particles pores diameter measured in the aforementioned way could be used to estimate the ratio between the particle diameter and pore size, $X = R_0/R_{pore,p}$. Unfortunately, from the SEM images, only the superficial pores can usually be seen (apart from few lucky exceptions as the one shown here), which might be sensibly different from the internal pores, as the pore diameter depends on the cooling rate, and this latter might change during the freezing process[37]. The external pore size is usually smaller, even more than one order of magnitude,

compared to the internal one. Moreover, the pore size can vary between particles (due to the different freezing conditions that each particle is subjected to) and, given the wide range of particles diameter that are usually obtained in a single experiment, X may vary as well in a wide range of values. For this reason, in the present study a parametric study was performed and X was varied in the range of 30 to 1000..

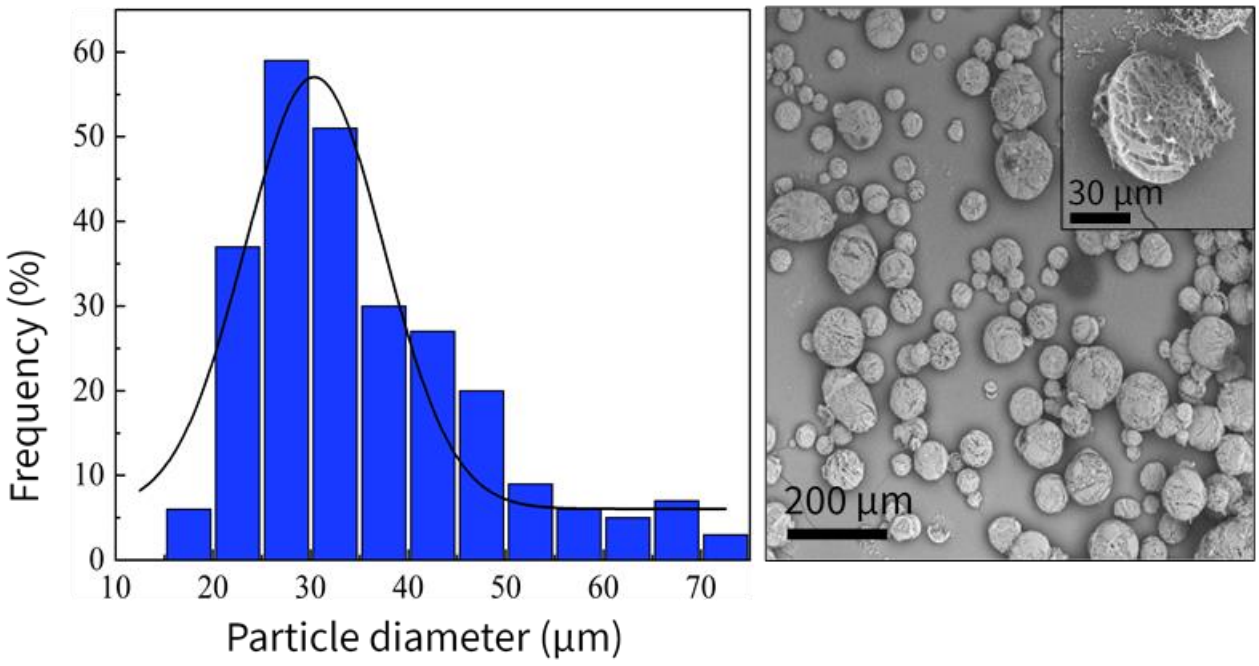

Figure 6. Particle size distribution and SEM images of a spray freeze-dried 5% (w/w) mannitol solution.

2.3.3. CASE STUDIES

Individual particle simulations were used to estimate the kinetic sublimation velocity v_s as a function of X, which was varied in the range between 5 and 1000. These values are representative of the system physical boundaries. When X=5 the particles pores diameter is comparable with the

particle itself and a further reduction would be impossible as no particle would exists. On the other hand, when X=1000, and for particles as the one described in section §2.3.2, the particles pores diameter reaches values lower then 30 nm, which is close to the the critical nucleus dimension during ice nucleation[38]. On the other hand, the physical properties of the packed bed were estimated using the methods described in §2.3.1. Three different functions were used as v_s, obtained from simulations at the microscopic scale respectively with a value of X=1000, X=100 and X=30. These three values represent three peculiar states of the system; the controlling resistance to mass transport in the system can either be determined by the particle, e.g. X=1000, the packed bed, e.g. X=30, or a combination of both, e.g. X=100. In all the simulations v_c was kept constant, i.e., 100 s^{-1}, while the other parameters and variables are listed in Table 1.

Table 1. List of all the parameters used in this work to define the system.

Parameter	Value/ Equation	Units
ΔH_s	2790.0	kJ/kg
$c_{p,ice}$	1967.8	J/kgK
$c_{p,gas}$	1674.7	J/kgK
$c_{p,s}$	$3.44\cdot10^{-3}T$+1.27	J/kgK
$c_{p,vial}$	840.0	J/kgK
k_{ice}	2.1	W/mK
k_{gas}	0.025	W/mK
k_s	$7.40\cdot10^{-3}T$+0.65	W/mK
k_{vial}	1.0	W/mK
ρ_{ice}	913	kg/m^3
ρ_{gas}	PM_w/(RT)	kg/m^3
ρ_s	1468	kg/m^3
ρ_{vial}	2600	kg/m^3
μ_{gas}	$18.46\cdot10^{-7}[T^{1.5}/(T$+650)]	Pas
M_w	18	g/mol
M_{in}	28.88	g/mol
ε_p	0.95	-
ε_{bed}	0.39	-
$B_{0,b}$	$1.11775\cdot10^{-11}$	m^2

$d_{pore,bed}$	19.5	μm
τ	1.33	-
P_c	15	Pa
T_{shelf}	-20 (single particle) 10 (packed bed)	°C
R_0	16.24	μm
R_{pore}	R_0/X	μm
A_1	5.07	W/m^2K
A_2	1.22	W/m^2KPa
A_3	0.021	1/Pa
$\varepsilon_{shelf,rad}$	0.3	-
$\varepsilon_{vial,rad}$	0.95	-
$\varepsilon_{bed,rad}$	0.9	-
T_0	-40	°C
Z_0	15	mm
Z_1	45	mm
$R_{out,vial}$	12	mm
$R_{in,vial}$	11	mm

2.3.4. SIMULATIONS

The simulations were carried out using the Finite Element Method (FEM) based sofware COMSOL Multiphysics version 5.6. At the microscopic level, the single particle was simulated as a 3D hemisphere while, at the macroscopic level, the system was simulated as a 2D-axisymmetric geometry as shown in Figure 2. An unstructured tetrahedral mesh was used for the individual particle, while for the particles bed (and vial), an unstructured triangular mesh was used. In both cases, a mesh independence study was performed by progressive refinement of the mesh, and the final mesh was chosen once the relative change (calculated on the average temperature and mass flux for the individual particles and local temperature and ice saturation for the particles bed) between consecutive mesh refinements was stable below 2%.

3. RESULTS

3.1.INDIVIDUAL PARTICLE ANALYSIS

We investigated the impact of the ratio between the particle diameter and pore size, X, on the drying behavior of individual particles so as to understand its effect on the kinetic parameter v_s. As X increases, the relative pore diameter in the individual particle decreases and, thus, the dried layer offers high resistance to vapor flow. The pressure gradient over the dried layer progressively increases to overcome this augmented resistance, and the particle temperature increases correspondingly. Depending on the value of X, two scenarios can occur. In the case of high values of X, the resistance to the vapor transport is high, and hence the particle temperature tends to approach the temperature of the heating source. In this case, the drying rate is controlled by the mass transfer within the particles. By contrast, if the values of X are small, the particle resistance to vapor flow is small and the water partial pressure at the sublimating interface approaches the pressure outside the particle. In this situation, the particle temperature equilibrates at the equilibrium temperature determined by the pressure outside the particle and, thus, the drying rate is controlled by heat transfer. These scenarios are shown in Figure 7a.

The kinetic parameter v_s strongly depends on the particle resistance to vapor flow, which depends on both X and the dried layer thickness. Figure 7b and 7c shows the dependence of v_s on X and S, respectively. If the value of X is experimentally determined, e.g., by SEM, the corresponding curve $v_s(S)$ in Figure 7b can be used as input to carry out simulations of the packed bed of particles.

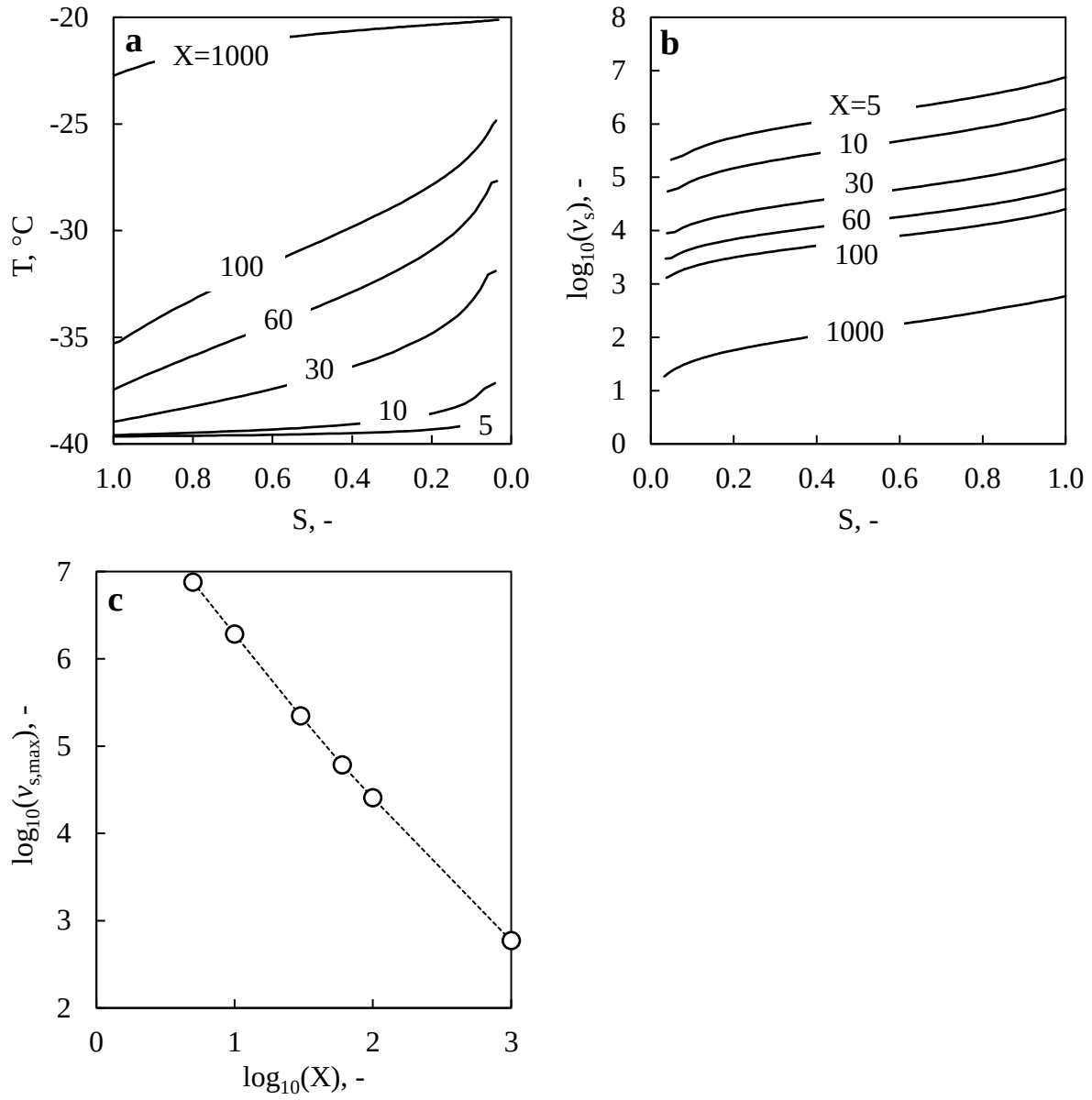

Figure 7. a) Average particle temperature as a function of X and S. **b)** Values of the kinetic parameter v_s (in logarithmic scale) as a function of X and S. **c)** Values of $v_{s,max} = v_s(S = 1)$ plotted against X on log-log scale.

3.2.PACKED BED SIMULATIONS

Once all the descriptors of the packed bed are defined, as well as the kinetic parameters, it is possible to simulate the drying of the packed bed of frozen particles. Figure 8 shows an example

of results for a packed bed of particles that resembles the real system described in section §2.3.2 and with a value of X equal to 100. The system was here described as a pseudo-homogenous medium and thus made of a single domain, but due to the steep gradient in the ice fraction S, it was still possible to distinguish the frozen and dried regions. This distinction, however, was not imposed a priori, as the previous mathematical models did[14,15], but resulted from the simulations. Moreover, three distinct sublimation fronts were noticeable. This phenomenon is peculiar to the drying of a packed bed of particles wherein all the particles are in direct contact with the vacuum environment independently of their position within the bed. The moving front at the bottom of the packed bed moved slowly upward because of the high resistance to vapor flow offered by the overlying particles. This last phenomenon prevailed and was only partially mitigated by the fact that particles closed to the bottom of the vial received the highest amount of heat, i.e., around 50% of the total energy. On the contrary, the top moving front was the fastest, although it received less than 40% of the total energy, i.e. radiation contribution from the top of the vial, thanks to lower packed bed resistance to vapor flow. Lastly, the third moving front appeared closed to the vial wall, and its formation was promoted by the vial wall itself which acted as a thermal fin.

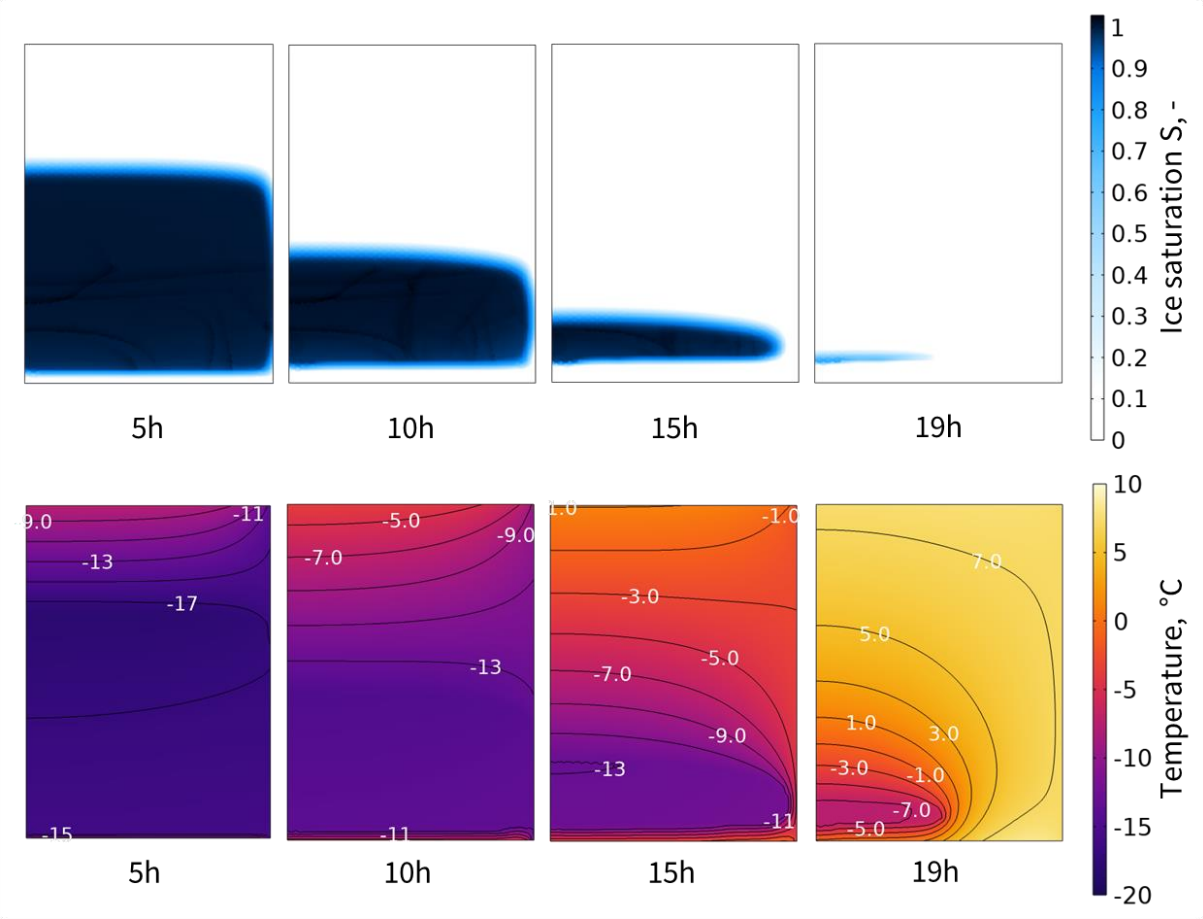

Figure 8. Evolution of the ice saturation and temperature contour plots of a packed bed of particles having X=100.

Independently of the particle morphology, two mechanisms contribute to the resistance to vapor flow, i.e. the resistance provided by the micro porosity of the particles and the one provided by the macro porosity of the packed bed. If X is small, e.g. $X \leq 30$, the mass transport resistance within the packed bed prevails over the individual particle resistance. In this case, i.e. X=30, we observed a sharp transition between high and low values of S as shown in Figure 9a and Figure 10. The diffused interface was localized within a region as thick as 0.1-0.3 mm, which corresponded to a few particles lined up. The diffused interface collapsed to a line and the result was very similar to those obtained by the simulation of conventional freeze-drying where the interface is solved as a

Stefan problem. However, even if similar, the diffused interface is able to predict the development of three simultaneous sublimation fronts, which is not possible in conventional freeze-drying. As the value of X increased, e.g. X=100, the particles mass transport resistance became comparable with the packed bed resistance and, consequently, the gradient in S became smoother. The diffused interface could be distinguished macroscopically and occupied a significant region of the packed bed as shown in Figure 9b. Eventually, for even higher values of X, e.g. X=1000, the drying rate is controlled by the mass transfer within the particle. It followed that ice sublimation occurred uniformly within the packed bed and the diffused interface occupied the whole bed, as shown in Figure 9c. Similar behavior is shown in Figure 11. At high values of X, all the particles started drying independently of their position within the packed bed; on the other hand, in the case of low values of X, the drying rate strongly depended on the particle position within the packed bed resulting in a sharp frozen-dried transition.

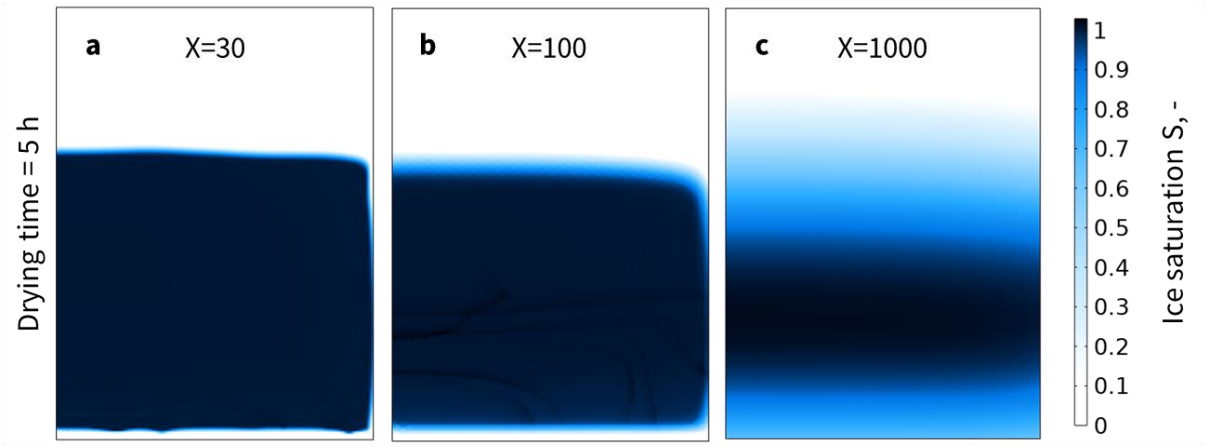

Figure 9. Ice saturation contour plots after 5h of drying for two packed beds characterized by the same macroscopic parameters with different microscopic structures.

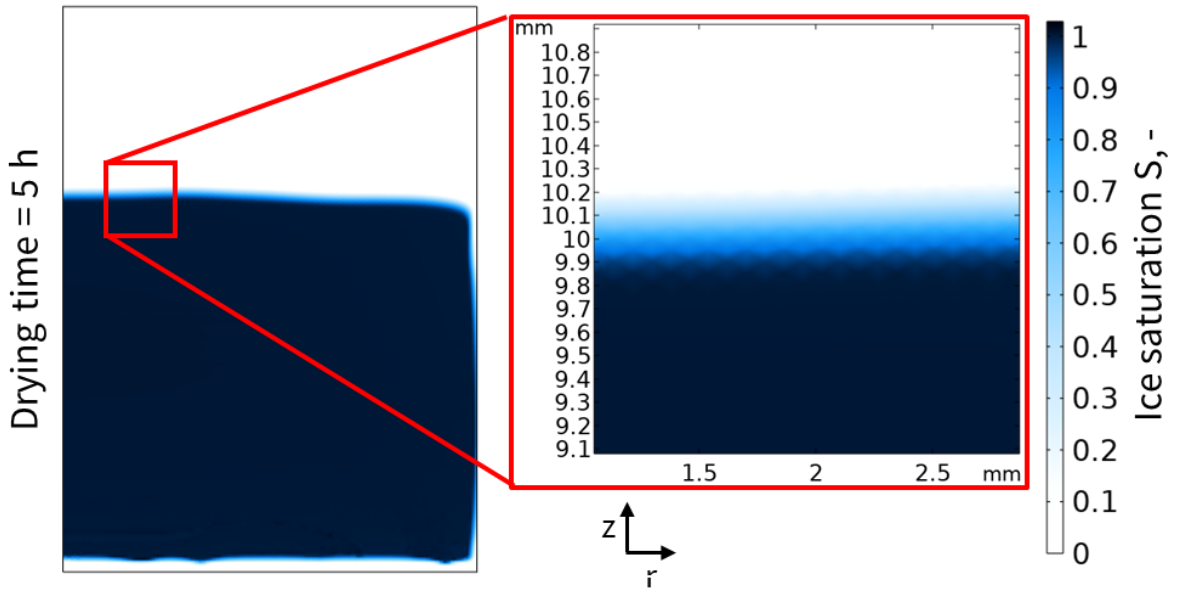

Figure 10. Ice saturation contour plots after 5h of drying for a packed bed with X=30 and magnification of the diffused interface. From the magnification it is possible to see that S dropped from 1 to 0 in the space of 0.2-0.3 mm.

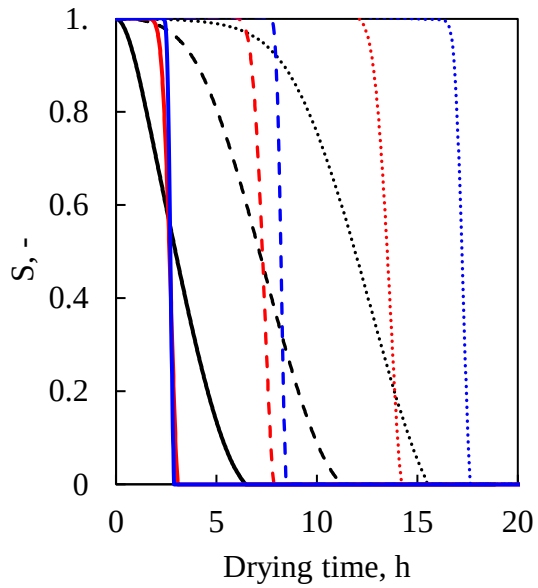

Figure 11. Ice saturation at different bed heights (solid lines z=12 mm, dashed lines z=8 mm and dotted line z=4 mm) over time for three packed beds having similar macroscopic structures but different microscopic characteristics (black: X =1000, red: X =100 and blue: X =30).

Further effects of the balance between the micro- and macro- mass transport resistance can be seen on the primary drying time and packed bed temperature. When the value of X was high, i.e. X=1000, the kinetic parameter v_s was small, as well as the sublimation flux in the single particle. Macroscopically, this low sublimation rate translated into a low level of water vapor in the packed bed, which could be expelled from the bed relatively quickly. The temperature of the system remained below -10°C and drying continued regularly until it ended in about 16 h. On the contrary, when the value of X was small, i.e. X=30, the sublimation flux inside the particle was high and water vapour accumulated within the packed bed, which represented the limiting resistance to the mass transport. When water vapor accumulated in the packed bed, the water pressure increased, and the packed bed temperature accordingly. Since the heating surfaces, i.e. the shelves, maintained a constant temperature throughout the whole process, the heat flux entering the system dropped, resulting in much slower drying, i.e. about 35 h. The behaviour here described and the temperature profiles of the simulations at X=30, 100 and 1000 are shown in Figure 12.

It can be noted that, while at the microscopic scale a high value of X corresponded to low sublimation rates and high particle temperatures and a low value of X corresponded to high sublimation rates and low particle temperature, the opposite happened at the macroscopic scale. At the microscopic scale, for low values of X, the particle temperature was determined by the pressure boundary condition, and it remained low as the pressure outside the particle remained low. However, in the packed bed, the sublimation flux produced at the microscopic scale influenced the pressure outside the particles. The result was a highly non-linear coupling of the

structures at the two scales. For a given particle size distribution and packing of the bed, the fastest drying is obtained by particles with a finer pore size.

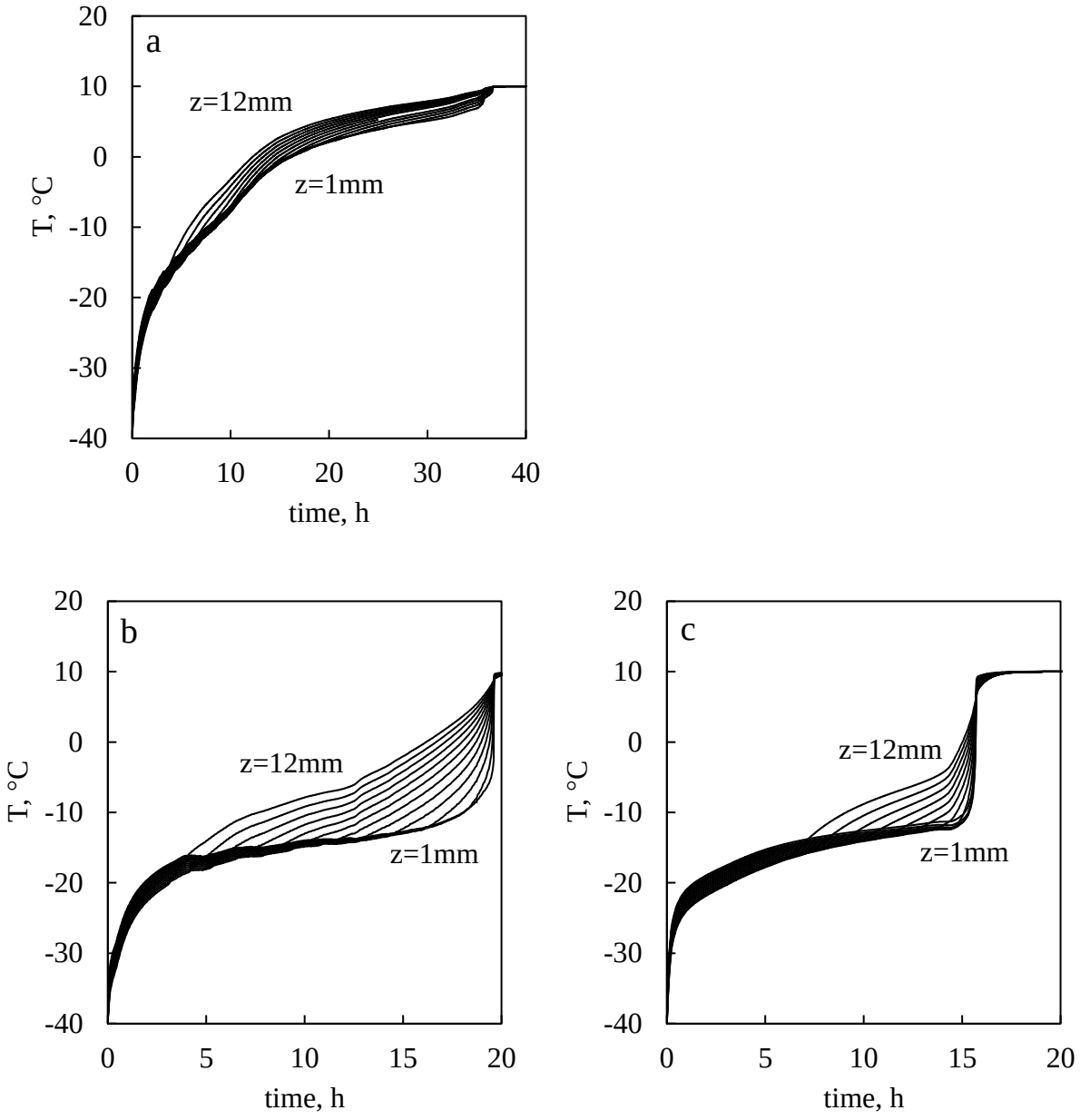

Figure 12. Temperature profiles of points located at r=0 and z varying from 1 mm to 12 mm (each line corresponds to a z increment of 1mm) for packed beds with the same macroscopic

structures but different microscopic ones: a) X=30, b) X=100 and c) X=1000. Note that in a) the x axis is twice as long as the one in b) and c).

4. CONCLUSIONS

A mathematical model was presented to describe the drying behavior of spray-frozen particles arranged in a packed bed. The model is based on the concept of a diffused interface and uses a multiscale approach to obtain the packed bed properties. Depending on the structure of the particles and the packed bed configuration, different scenarios can occur. For example, when the mass transport resistance inside the packed bed is higher than inside the individual particle, a steep transition between the partially and fully dried particles appears. In comparison, when the resistance inside the single particle is higher than that of the packed bed, sublimation uniformly starts within the entire packed bed, and no sharp transition can be detected. Moreover, the drying time of the bed is influenced by the microscopic structure of the particles and the longest drying times are observed for particles with the biggest pores.

The present method overcomes the inaccuracies of the previous ones found in the literature and can predict behaviors that could not have been detected before, i.e. multiple drying fronts. For this reason, it can be of great help in the development of spray freeze drying cycles and drugs preparation. However, a detailed experimental validation is still necessary to test the model and to further understand the drying of packed beds. The temperature measurements are complicated as common thermocouples fail to give accurate readings when they are in contact with different materials at the same time, e.g., solid particles and water vapor. The use of infra-red thermography might be of incredible help in the inspection of these systems and this technology recently demonstrated to be a useful tool in doing so for freeze-dried solutions in bulk[7,8,39–41]. Unfortunately, other problems should be solved to be able to apply it to spray freeze drying, i.e.,

the glass of common vials is opaque to the infra red rations and the temperature of the container surface can vary by several degrees from the packed bed temperature. Moreover, the internal temperature of the packed bed would still remain inaccessible. Moreover, the internal structure of the single particles is almost inaccessible due to their small dimension, but the packed beds are incredibly sensitive to this characteristic, as shown in this paper. Future developments of this work might even go in the direction of inferring the internal structure of the particles by the analysis of macroscopic parameters like the primary drying time, which is straightforward to determine. However, to do so it is necessary to have detailed information on the heat transfer coefficient involved in the process since it would not be possible to determine it using the drying time as done in the present paper. Several points worth being further elaborated, but this model is a useful starting point to gain insight into the spray freeze drying process and support its application in the pharmaceutical industry.

AUTHOR INFORMATION

Corresponding Authors

Roberto Pisano – Molecular Engineering Laboratory (molE), Department of Applied Science and Technology, Politecnico di Torino, 24 corso Duca degli Abruzzi, IT-10129 Torino, Italy.. Email: roberto.pisano@polito.it.

ACKNOWLEDGEMENTS

Computational resources were provided by HPC@polito, which is a project of Academic Computing within the Department of Control and Computer Engineering at the Politecnico di Torino (http://www.hpc.polito.it

AUTHOR CONTRIBUTIONS

Editing (LS, MBA, AM, GB, RP), Revision (LS, MBA, AAB, AM, GB, RP), data analysis (LS, RT, MBA, AM, GB, RP), supervision (GB, RP).

FUNDING SOURCES

This research had no external funding sources.

ABBREVIATIONS

DGM, Dusty Gas Model; SFD, Spray Freeze Drying; SEM, Scanning Electron Microscope.

REFERENCES

1. Market and Markets. Freeze-Drying/ Lyophilization Market by Type (Tray, Shell, Manifold), Scale of operation (Industrial, Lab, Pilot), Application (Food, Pharma & Biotech), Accessories (Loading & Unloading, Monitoring, Vacuum Systems) - Global Forecast to 2025. *B2B Reports PH2704* (2021).

2. Langford, A., Bhatnagar, B., Walters, R., Tchessalov, S. & Ohtake, S. Drying technologies for biopharmaceutical applications: Recent developments and future direction. *Dry. Technol.* **36**, 677–684 (2018).

3. Stratta, L., Capozzi, L. C., Franzino, S. & Pisano, R. Economic Analysis of a Freeze-Drying Cycle. *Processes* **8**, 1399 (2020).

4. Pisano, R., Arsiccio, A., Capozzi, L. C. & Trout, B. L. Achieving continuous manufacturing in lyophilization: Technologies and approaches. *European Journal of Pharmaceutics and Biopharmaceutics* vol. 142 (2019).

5. Capozzi, L. C., Trout, B. L. & Pisano, R. From Batch to Continuous: Freeze-Drying of Suspended Vials for Pharmaceuticals in Unit-Doses. *Ind. Eng. Chem. Res.* **58**, 1635–1649 (2019).

6. Leys, L. *et al.* A primary drying model-based comparison of conventional batch freeze-drying to continuous spin-freeze-drying for unit doses. *Eur. J. Pharm. Biopharm.* **157**, 97–107 (2020).

7. Van Bockstal, P.-J. *et al.* Developing a framework to model the primary drying step of a continuous freeze-drying process based on infrared radiation. *Eur. J. Pharm. Biopharm.* **127**, 159–170 (2018).

8. Van Bockstal, P.-J., Corver, J., De Meyer, L., Vervaet, C. & De Beer, T. Thermal Imaging as a Noncontact Inline Process Analytical Tool for Product Temperature Monitoring during Continuous Freeze-Drying of Unit Doses. *Anal. Chem.* **90**, 13591–13599 (2018).

9. De Meyer, L. *et al.* Evaluation of spin freezing versus conventional freezing as part of a continuous pharmaceutical freeze-drying concept for unit doses. *Int. J. Pharm.* **496**, 75–85 (2015).

10. Maa, Y. F., Nguyen, P. A., Sweeney, T., Shire, S. J. & Hsu, C. Protein inhalation powders: Spray drying vs spray freeze drying. *Pharmaceutical Research* vol. 16 249–254 (1999).

11. Isleroglu, H., Turker, I., Tokatli, M. & Koc, B. Ultrasonic spray-freeze drying of partially purified microbial transglutaminase. *Food Bioprod. Process.* **111**, 153–164 (2018).

12. Adali, M. B., Barresi, A. A., Boccardo, G. & Pisano, R. Spray Freeze-Drying as a Solution to Continuous Manufacturing of Pharmaceutical Products in Bulk. *Processes* **8**, 709 (2020).

13. Sharma, A., Khamar, D., Cullen, S., Hayden, A. & Hughes, H. Innovative Drying

Technologies for Biopharmaceuticals. *Int. J. Pharm.* **609**, 121115 (2021).

14. Liapis, A. I. & Bruttini, R. A mathematical model for the spray freeze drying process: The drying of frozen particles in trays and in vials on trays. *Int. J. Heat Mass Transf.* **52**, 100–111 (2009).

15. Capozzi, L. C., Barresi, A. A. & Pisano, R. A multi-scale computational framework for modeling the freeze-drying of microparticles in packed-beds. *Powder Technol.* **343**, 834–846 (2019).

16. Capozzi, L. C., Barresi, A. A. & Pisano, R. Supporting data and methods for the multi-scale modelling of freeze-drying of microparticles in packed-beds. *Data Br.* **22**, 722–755 (2019).

17. Mason, E. A., Malinauskas, A. P. & Evans, R. B. Flow and Diffusion of Gases in Porous Media. *J. Chem. Phys.* **46**, 3199–3216 (1967).

18. Pisano, R., Fissore, D. & A., A. Heat Transfer in Freeze-Drying Apparatus. in *Developments in Heat Transfer* (InTech, 2011). doi:10.5772/23799.

19. Pisano, R., Fissore, D. & Barresi, A. A. In-Line and Off-Line Optimization of Freeze-Drying Cycles for Pharmaceutical Products. *Dry. Technol.* **31**, 905–919 (2013).

20. Velardi, S. A. & Barresi, A. A. Development of simplified models for the freeze-drying process and investigation of the optimal operating conditions. *Chem. Eng. Res. Des.* **86**, 9–22 (2008).

21. Reitzle, M. *et al.* Direct numerical simulation of sublimating ice particles. *Int. J. Therm. Sci.* **145**, 105953 (2019).

22. Marti, J. & Mauersberger, K. A survey and new measurements of ice vapor pressure at temperatures between 170 and 250K. *Geophys. Res. Lett.* **20**, 363–366 (1993).

23. Smilauer et al. Yade Documentation 3rd ed. (2021) doi:10.5281/zenodo.5705394.

24. Cundall, P. A. & Strack, O. D. L. A discrete numerical model for granular assemblies. *Géotechnique* **29**, 47–65 (1979).

25. Bear, J. *Dynamics of Fluids in Porous Media*. (Dover publications, 1988).

26. Marcato, A., Boccardo, G. & Marchisio, D. From Computational Fluid Dynamics to Structure Interpretation via Neural Networks: An Application to Flow and Transport in Porous Media. *Ind. Eng. Chem. Res.* **61**, 8530–8541 (2022).

27. Marcato, A., Boccardo, G. & Marchisio, D. A computational workflow to study particle transport and filtration in porous media: Coupling CFD and deep learning. *Chem. Eng. J.* **417**, 128936 (2021).

28. Sobieski, W. Calculating the binary tortuosity in DEM-generated granular beds. *Processes*

8, (2020).

29. Koponen, A., Kataja, M. & Timonen, J. Tortuous flow in porous media. *Phys. Rev. E* **54**, 406–410 (1996).

30. Duda, A., Koza, Z. & Matyka, M. Hydraulic tortuosity in arbitrary porous media flow. *Phys. Rev. E* **84**, 036319 (2011).

31. Gostick, J. *et al.* PoreSpy: A Python Toolkit for Quantitative Analysis of Porous Media Images. *J. Open Source Softw.* **4**, 1296 (2019).

32. Adali, M. B., Barresi, A., Boccardo, G., Montalbano, G. & Pisano, R. Ultrasonic spray freeze-drying of sucrose and mannitol-based formulations: Impact of the atomization conditions on the particle morphology and drying performance. *Dry. Technol.* **0**, 1–11 (2022).

33. Bruttini, R. & Liapis, A. I. The drying rates of spray freeze drying systems increase through the use of stratified packed bed structures. *Int. J. Heat Mass Transf.* **90**, 515–522 (2015).

34. Malecki, G. J., Shinde, P., Morgan, A. I., & Farkas, D. F. Atmospheric fluidized bed freeze drying. *Food Technol.* 601–603 (1970).

35. Ishwarya, S. P., Anandharamakrishnan, C. & Stapley, A. G. F. Spray-freeze-drying: A novel process for the drying of foods and bioproducts. *Trends Food Sci. Technol.* **41**, 161–181 (2015).

36. Pisano, R. Automatic control of a freeze-drying process: Detection of the end point of primary drying. *Dry. Technol.* **0**, 1–18 (2020).

37. Arsiccio, A., Barresi, A. A. & Pisano, R. Prediction of Ice Crystal Size Distribution after Freezing of Pharmaceutical Solutions. *Cryst. Growth Des.* **17**, 4573–4581 (2017).

38. Bai, G., Gao, D., Liu, Z., Zhou, X. & Wang, J. Probing the critical nucleus size for ice formation with graphene oxide nanosheets. *Nature* **576**, 437–441 (2019).

39. Lietta, E., Colucci, D., Distefano, G. & Fissore, D. On the Use of Infrared Thermography for Monitoring a Vial Freeze-Drying Process. *J. Pharm. Sci.* **108**, 391–398 (2019).

40. Harguindeguy, M., Stratta, L., Fissore, D. & Pisano, R. Investigation of the Freezing Phenomenon in Vials Using an Infrared Camera. *Pharmaceutics* **13**, 1664 (2021).

41. Harguindeguy, M., Stratta, L., Fissore, D. & Pisano, R. Combining Mathematical Modeling and Thermal Infrared Data in the Freezing of Pharmaceutical Liquid Formulations. (2022) doi:10.1021/acs.iecr.1c04595.

42. Abbas, M. N. Modeling Of Porosity Equation For Water Flow Through Packed Bed Of Monosize Spherical Packing. **15**, 205–226 (2011).